Applied Ocean Research 43 (2013) 166–174

Contents lists available at ScienceDirect

Applied Ocean Research

journal homepage: www.elsevier.com/locate/apor

Time domain prediction approach for cross-flow VIV induced fatigue damage of steel catenary riser near touchdown point

Kunpeng Wang, Hongxiang Xue*, Wenyong Tang

State Key Laboratory of Ocean Engineering, Shanghai Jiao Tong University, Shanghai 200240, China

ARTICLE INFO

Article history:
Received 4 March 2013
Received in revised form 6 September 2013
Accepted 11 September 2013

Keywords:
Vortex-induced vibration
SCR–soil interaction
Trench shape
Touchdown point
Soil suction
Fatigue damage

ABSTRACT

Previous steel catenary riser (SCR) models targeted for VIV prediction are truncated at touchdown point (TDP) where simple constrain and rotation stiffness are generally applied. In this study, a time domain approach accounting for the SCR–soil interaction is proposed to predict the cross-flow (CF) VIV induced fatigue damage of a SCR near TDP. The hydrodynamic force is simulated based on the forced vibration test data as a function of the non-dimensional amplitude and frequency, and an empirical damping model. When the non-dimensional frequency associated with the calculated frequency falls in the excitation region, the natural frequency closer to the frequency corresponding to the maximum excitation force is taken to be the dominant frequency, and applied to obtain the excitation force. The SCR–soil interaction model takes into account the trench shape, and the mobilization and release of the soil suction. Fatigue damage is linearly accumulated by using the rain-flow counting methodology. To validate the proposed models, simulation for a riser model test is carried out, and the envelopes of RMS displacement, curvature, and fatigue damage are compared. Further works focus on the sensitivity of VIV induced fatigue damage near TDP to the seabed parameters, such as mudline shear strength, shear strength gradient and soil suction, and some conclusions are obtained.

1. Introduction

Steel catenary risers (SCRs) are considered to be technically feasible and commercially efficient solutions for deepwater oil and gas productions, and used extensively in recent years [1,2]. However, due to its slender feature and particular configuration, the designer still encounter some challenging issues affecting the fatigue life of a SCR. When a riser is exposed to ocean current, periodic vortex shedding occurs at the two sides of the riser. This can cause the riser vibration, namely VIV. When the vortex shedding frequency and the riser response frequency are locked in, the riser response would be severely magnified, which may cause fatigue damage accumulation. Touchdown point (TDP) where SCR starts to contact the seabed is one of the critical positions prone to fatigue failure. Therefore, it is essential to predict the VIV response near TDP accurately in a SCR design.

VIV is a complex fluid–structure interaction phenomenon. The studies for VIV mainly focused on the laboratory test of rigid cylinder in the initial stage to capture the particular phenomena and characteristics [3–5]. Based on these tests, some frequency domain codes for VIV assessment have been developed, such as Shear7 [6] and VIVANA [7], and are widely used in the riser design by using large safety factor [8]. Frequency domain approach can economize the computational time, but cannot account for the variation of current, the soil–SCR interaction and some other nonlinear boundary conditions. Therefore, many recent studies focus on the time domain method. Finn et al. [9] and Grant et al. [10] developed the time domain code, ABAVIV, to simulate the intermittent VIV phenomena observed in a Joint Industry Project [11]. This code is based on the finite element package ABAQUS and uses user subroutine to connect the riser response with hydrodynamic force model in Blevins [12]. Cheng et al. [13–15] carried out the validation works using different riser models, and found that ABAVIV can well capture the higher harmonics response which frequency domain approach fails to achieve. According to forced algorithm, Ma and Qiu [16] used forced vibration test data [17,18] to predict CF-VIV of the riser test model in Chaplin et al. [19,20] in time domain. Sidarta et al. [21] developed VIV time domain prediction code, SimVIV also based on ABAQUS by implanting the lift coefficient used in Shear7 version 4.2-f [6]. Wang et al. [22] proposed a time domain approach using a new VIV lock-in criterion and preliminarily validated it by comparing with the model tests.

Time domain VIV studies mainly focus on top tension risers (TTRs), and only few works [23] are on the investigation of SCRs. Larsen and Passano [23] pointed out that the predicted VIV induced fatigue damages using truncation SCR and full SCR considering touchdown zone are obviously different. Therefore, it is necessary to combine a time domain VIV model and a reasonable SCR–soil interaction model to simulate the response near TDP. Actually, many studies for the SCR–soil interaction mechanics have been carried out and proposed some practical models. Based on the STRIDE and CARISIMA JIPs [24,25],

* Corresponding author at: No. 800, Dongchuan Road, School of Naval Architecture, Ocean & Civil Engineering, Shanghai Jiao Tong University, Shanghai 200240, China. Tel.: +86 21 34204968; fax: +86 21 34206642.
E-mail address: hongxiangxue@sjtu.edu.cn (H. Xue).

0141-1187/$ - see front matter © 2013 Elsevier Ltd. All rights reserved.
http://dx.doi.org/10.1016/j.apor.2013.09.003

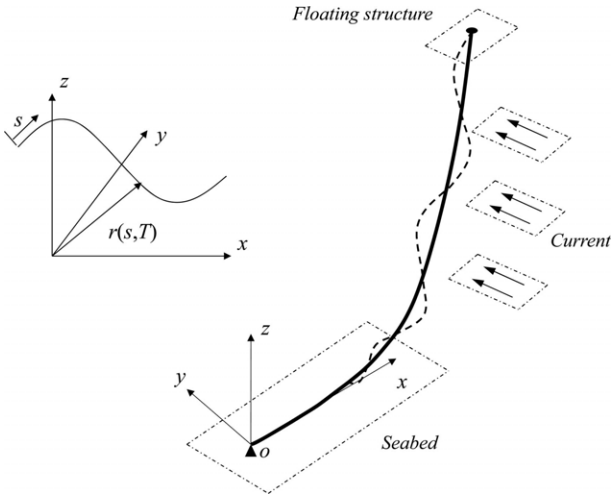

Fig. 1. A model of SCR subjected to current flow.

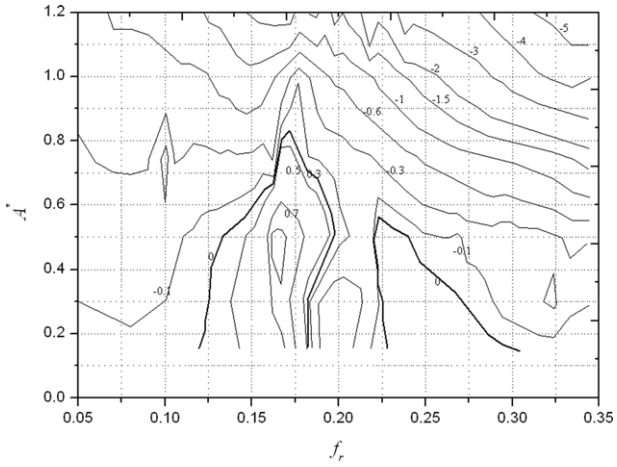

Fig. 2. Contour plot of the lift coefficient, C_V [4].

Bridge and Laver [26] proposed the conservative large displacement soil stiffness model and soil stiffness model considering soil suction force. Aubeny et al. [27] used the backbone curve and beam-spring model to obtain the riser shape near the touchdown zone (TDZ), and depicted the SCR–soil interaction by nonlinear hysteretic model including four stages: re-contact, elastic rebound with full soil–pipe contact, partial soil–pipe separation and full separation, see Fig. 4. Nakhaee and Zhang [28] implanted the nonlinear hysteretic model into finite element code, CABLE3D, and discussed the trench development and its feedback effect on the bending moment near TDP. Wang et al. [29] linearized the hysteretic model and studied the effects of the seabed parameters on the fatigue damage near TDP. It should be noted that although the SCR–soil interaction has been extensively investigated, previous studies [30–32] usually employ the truncation model with simple constrain at TDP, and some characteristics of VIV response near TDP may be hardly obtained.

The objective of this paper is to develop an approach for the VIV prediction of SCRs, and further investigate the effect of seabed parameters on the VIV induced fatigue damage near TDP. All works cover the following parts. Firstly, a time domain code for VIV prediction is developed, using the forced vibration test data [4] and an empirical damping model [33] to simulate the hydrodynamic force. Secondly, a linear hysteretic model and a trench shape model are proposed to model the SCR–soil interaction and rain-flow counting methodology

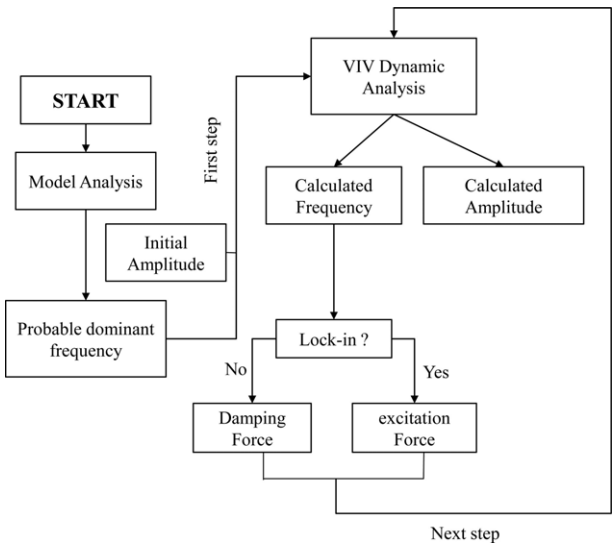

Fig. 3. Flowchart of VIV analysis.

is introduced to calculate the fatigue damage. Then, the proposed approach is validated by comparing with the RMS displacement, curvature, and the fatigue damage of the riser model experiment. Furthermore, parametric studies are carried out to quantify the sensitivity of the fatigue damage near TDP to seabed parameters.

2. VIV prediction model

2.1. Model formulation

SCR is a nonlinear slender structure with particular configuration. Fig. 1 shows a model of SCR including the TDZ in the global Cartesian coordinate system and a riser element in curvilinear coordinate system. Considering high aspect ratio of length to diameter, SCR response can be depicted by the following differential equation:

$$\rho\ddot{r} + c\dot{r} + (EIr'')'' - (T_e r')' = F_f + F_s \tag{1}$$

where r is the position vector, dots and primes denote differentiation with respect to time T and arc length s respectively. ρ is the riser mass per unit length, c is the structural damping, E is the elastic modulus, I is the moment of inertia, T_e is the effective tension, F_f is the hydrodynamic force, and F_s is the seabed resistance.

As regards to VIV analysis, the hydrodynamic forces associated with vortex shedding are generally decomposed into two components: excitation force, F_V in phase with riser velocity, and inertia force, F_M in phase with riser acceleration [34]. By assuming that the riser yields to sinusoidal response, they can be expressed as:

$$F_V = \frac{1}{2} C_V(A^*, f_r)\rho_f D V^2 \cos(\omega T) \tag{2}$$

$$F_M = \frac{\pi}{4} C_M(A^*, f_r)\rho_f D^2\omega^2 A \sin(\omega T) = -m_a\ddot{r} \tag{3}$$

where $C_V(A^*, f_r)$ and $C_M(A^*, f_r)$ are excitation coefficient and added mass coefficient, $A^* = A/D$ is the non-dimensional amplitude, $f_Y = fD/V$, f is the dominant frequency of riser's response, ρ_f is the fluid density, D is the riser diameter, V is the current velocity, A is the response amplitude, ω is the circular frequency, and m_a is the added mass per unit length.

In this study, the forced vibration test data of rigid cylinder [4] are applied for the hydrodynamic force. Fig. 2 gives the contour of C_V as functions of A^* and f_Y. Positive coefficient means excitation force synchronizes to the riser motion, whereas negative values mean hydrodynamic damping. The corresponding damping coefficient is

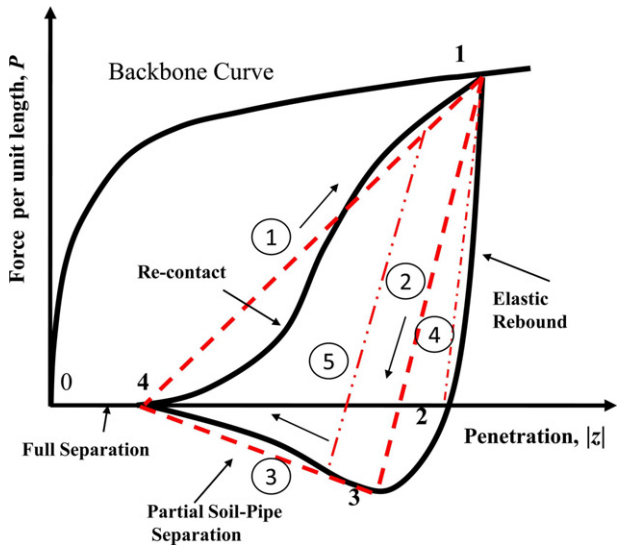

Fig. 4. SCR–soil interaction model.

obtained according to the equivalent dissipated power:

$$c_f = -\frac{C_V \rho_f V^2 D}{2A\omega} \tag{4}$$

Outside the test range defined by f_r in Fig. 2, the empirical damping model proposed by Venugopal [33] widely used in the frequency domain code [6,7], is applied to model the hydrodynamic damping. For the completeness, it is briefly described below.

High non-dimensional frequency damping model:

$$c_f = C_{lf}\rho_f DV + c_{sw} \tag{5}$$

where C_{lf} is an empirical coefficient taken to be 0.18. c_{sw} is the still water contribution given by:

$$c_{sw} = \frac{\omega\pi\rho_f D^2}{2}\left[2\sqrt{\frac{2}{\omega D^2/\nu}} + C_{sw}\left(\frac{A}{D}\right)^2\right] \tag{6}$$

where ν is the kinematic viscosity of the fluid, and C_{sw} is an empirical coefficient taken to be 0.2.

Low non-dimensional frequency damping model:

$$c_f = \frac{C_{hf}\rho_f V^2}{\omega} \tag{7}$$

where C_{hf} is an empirical coefficient taken to be 0.2.

2.2. Determination of amplitude and dominant frequency

As shown in Fig. 2, VIV response has an excitation region determined by non-dimensional frequency. In VIVANA [7], its bandwidth is defined from 0.125 to 0.2, which is corrected for the variation of Strouhal frequency according to Eq. (8). In this region, the non-dimensional frequency corresponding to the maximum excitation force approximately allows for the largest amplitude. This study considers the point as the power-in center.

$$\left(\frac{f_r}{S_t}\right)_{test} = \left(\frac{f_r}{S_t}\right)_{actual} \tag{8}$$

For each element, the most probable dominant frequency is preliminary defined by the natural frequency closer to power-in center. By assigning an initial amplitude and the probable dominant frequency to each element, the hydrodynamic force can be calculated to drive the oscillation of the SCR. At each calculation step, the displacement, velocity and time are extracted to update the amplitude and frequency. It should be noted that this frequency is named by calculated frequency, not the dominant frequency.

If the calculated non-dimensional frequency falls in the excitation region, lock-in would occur and the most probable dominant frequency would be assumed to the actual dominant frequency; if not, the calculated frequency would be considered as the dominant frequency. Once the dominant frequency and amplitude are determined, the hydrodynamic force can be calculated for the next step VIV analysis. The flowchart of the VIV analysis is shown in Fig. 3.

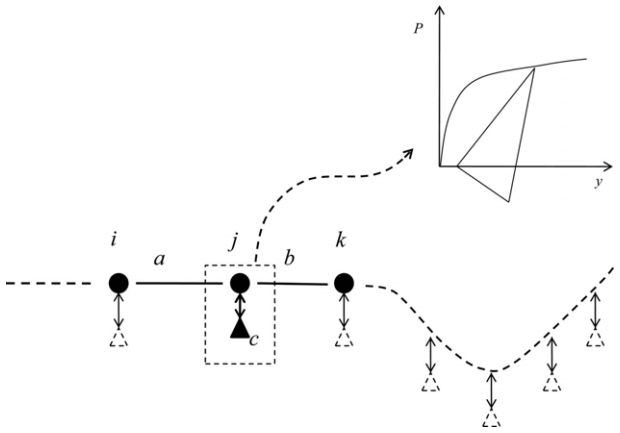

Fig. 5. Sketch of TDZ element connected with SCR.

3. SCR–soil interaction model

The nonlinear hysteretic model proposed by Aubeny et al. [27] is shown as the black solid curve in Fig. 4. It is seen that the soil resistance is changed to suction when the SCR moves upwards. Compared with the conservative large displacement soil stiffness model and soil stiffness model considering soil suction force [26] depicted by dot dash line ④and dash line ②respectively in Fig. 4, this model well describes the SCR–soil interaction process: loading–unloading–reloading.

This study proposes a linear SCR–soil interaction model as showed in Fig. 4, following the enclosed dash line (①→ ②→ ③), which is determined by three points: trench depth point 1, maximum suction point 3 and SCR–soil separation point 4. According to the model, a single point TDZ element is created in the finite element code. Fig. 5 shows the TDZ element c connected with beam element a and b by node j. In a response loop, when node j penetrates into remoulded seabed, TDZ element applies upward resistance to SCR. The resistance increases to the maximum at point 1, and then decreases along dash line ②, and further changes to soil suction. For the case that the node j moves upwards without arriving at point 1, the P–$|z|$ relation is assumed to follow a straight line parallel to dash line ②, such as double dot dash line ⑤.

Continuous impact of a SCR can cause seabed plastic deformation with trench development. Trench depth is not uniform along TDZ. In Bridge and Howells [35], the trench is observed as ladle shaped in profile, and the SCR is in general considered to include three zones: catenary zone, buried zone and surface zone, as shown in Fig. 6.

At the surface zone, the trench depth is the self-weight penetration against the virgin seabed with the resistance, P following the backbone curve expressed as follows [27]:

$$P = N_P D\,(S_0 + S_g\,|z|) \tag{9}$$

where N_P is a dimensionless bearing factor, S_0 and S_g are mudline shear strength and shear strength gradient respectively.

According to the observed shape, the trench corresponding to the buried zone is simplified to linear and nonlinear zones. As an attempt, the horizontal length l_B and l_L, and the slope angle α of the linear zone

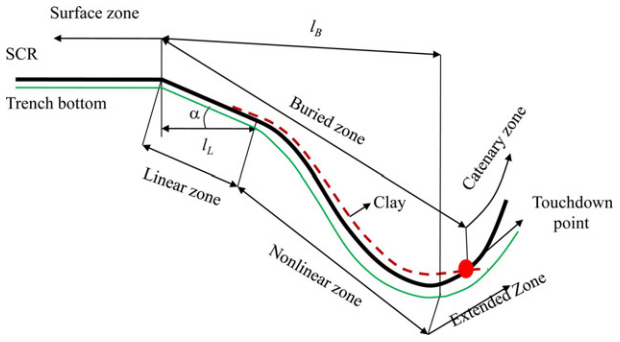

Fig. 6. Sketch of trench shape.

Table 1
Parameters of SCR–soil interaction model.

Particulars	Definition
$\|z\|_{\max}$	Maximum depth of trench for beam-spring model
S_0	Seabed mudline shear strength
S_g	Seabed shear strength gradient
μ_{sep}	Riser-soil separation factor $\|z\|_4/\|z\|_1$
λ_{suc}	Position factor of maximum suction $(\|z\|_3 - \|z\|_4)/(\|z\|_1 - \|z\|_4)$
f_{suc}	Maximum suction factor $-P_3/P_1$
γ	Empirical parameter for trench shape
φ	Empirical parameter for trench shape
β	Empirical parameter for trench shape

are given as:

$$\begin{aligned} l_B &= \gamma\sqrt{|z|_{\max}/D}/\rho^{1/3} \\ l_L &= \frac{\sqrt{|z|_{\max}/D}}{1+\varphi\sqrt{|z|_{\max}/D}}\varphi l_B \\ \alpha &= atg\left(\beta\sqrt{|z|_{\max}/D}\right) \end{aligned} \tag{10}$$

where $|z|_{max}$ is the maximum penetration in a trench, γ, φ and β are empirical parameters.

The nonlinear zone is described as the following linear differential equation by assuming the balance of the riser weight and seabed resistance:

$$\frac{d^4|z|}{dx^4} = 0 \tag{11}$$

By applying the same trench depth and rotation angle with the linear zone at left end, and maximum trench depth and zero rotation angle at the right end, the nonlinear zone shape can be obtained.

In general, due to the slow-drift motion of the upper end, the trench often has a long extended zone at the right side of the maximum penetration position. For simplification, this zone is considered as the mirror symmetry of the nonlinear zone with respect to the maximum penetration position.

According to the calculated trench shape, the penetration and the associated seabed resistance at point 1 are obtained. The seabed suction has significant relationship with point 3 determined by two parameters: λ_{suc} for penetration corresponding to the maximum suction, and f_{suc} for the maximum suction. Point 4 is the SCR–soil separation position, determined by parameter μ_{sep}. As a summary, the parameters of SCR–soil interaction model are presented in Table 1.

4. Methodology for fatigue damage

The most common approach for the assessment of riser fatigue is S–N approach. It assumed that the riser material performance is well depicted by the S–N equation as follows [36]:

$$N = A\left[\Delta S \cdot SCF \cdot \left(\frac{t}{t_{ref}}\right)^k\right]^{-m} \tag{12}$$

where N is the permissible number of cycles when applying stress with a range of ΔS in MPa, SCF is the stress concentration factor, A and m are material constants, t/t_{ref} is the thickness correction factor, the reference thickness t_{ref} equals 25 mm. In this study, the related parameters are taken as: $m = 3$, $\lg A = 11.687$, SCF = 1.0 [36].

The rain-flow counting methodology is applied to obtain the stress range according to the time history of the stress given as the combination of the axial (σ_a) and bending stress (σ_M):

$$\sigma = \sigma_a + \sigma_M \tag{13}$$

Based on the stress range, the fatigue damage could be calculated by using the Palmgren–Miner linear damage accumulation hypothesis (Miner's rule):

$$D_{acc} = \sum_{i=1}^{N} \frac{n_i}{A\left[\left(\Delta S_i \cdot SCF \cdot (t/t_{ref})^k\right)\right]^{-m}} \tag{14}$$

where N represents the number of different stress cycles, n_i is the number of the stress cycle with a range of ΔS_i in MPa, and D_{acc} is the accumulated fatigue damage.

5. Validation

5.1. Validation for VIV prediction model and fatigue damage methodology

Validation work is carried out using the HanØtangen riser model [37,38], which has the following parameters: the length $L = 90$ m, the outer diameter $D = 0.03$ m, the inner diameter $D_{in} = 0.026$ m, mass ratio of riser to displacement water is 3.13, top tension is 3700 N. The Strouhal number is taken to be 0.19 in the numerical simulation.

The test was done under several cases with linearly sheared current velocity varying from 0.16 m/s to 1.96 m/s at riser top end. The comparison for the VIV response is carried out by using the case with maximum current of 0.54 m/s. Fig. 7 illustrates the amplitude spectrum of midpoint numerically and experimentally obtained. It is noted that the proposed model predicts excited mode frequencies from 2 to 3 Hz similar to the test results [38], but predicts fewer excited frequencies. Therefore, the response is more regular than the measured data, as shown in Fig. 8. However, the displacement is almost in the same region from −0.015 m to 0.015m for both models. The ratio of RMS displacement to diameter along the riser is demonstrated in Fig. 9. At the lower end, the present results shows well agreement with the test data, but at the upper end, is over estimated. Additionally, the trend of the envelopes shows good accordance.

To validate the fatigue damage methodology, the numerically and experimentally obtained fatigue damages for the case with maximum current of 0.64 m/s are shown in Fig. 10. Overall, the results show well agreement, especially at the bottom zone.

5.2. Validation for SCR–soil interaction model

Bridge and Howells [35] reported the observed trenches of several SCRs at the Allegheny and Marlin of GoM. This study selects the trenches of oil and gas export SCRs at Allegheny to validate the proposed trench model. The two SCRs have the same dimensional parameters: $D = 0.3239$ m, $D_{in} = 0.2889$ m. The parameters m and $|z|_{max}$ are 182 kg and 2.1 riser diameters for oil export SCR, and are 132 kg and 4.3 riser diameters for gas export SCR. By matching numerically obtained trenches with the field observations, the parameters

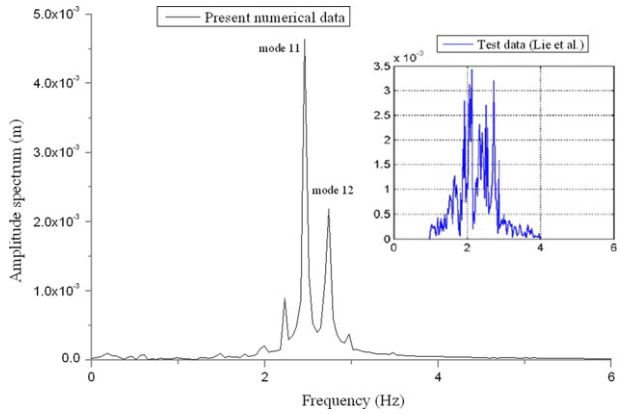

Fig. 7. Amplitude spectrum of midpoint.

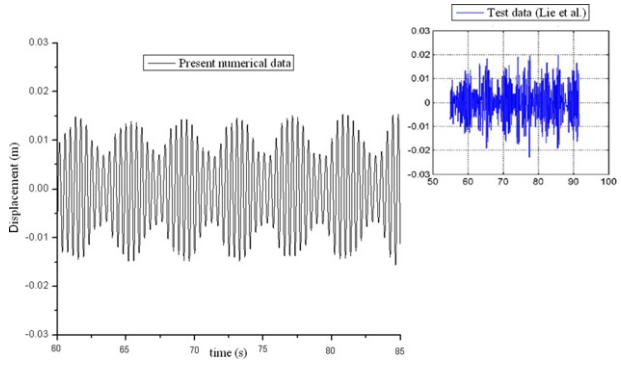

Fig. 8. Displacement response of midpoint.

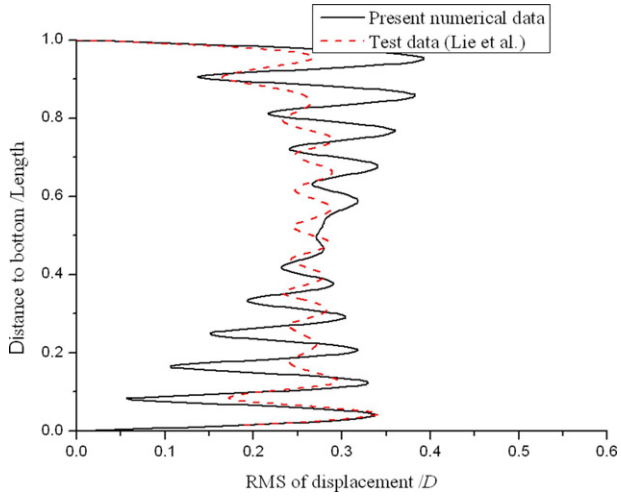

Fig. 9. RMS of displacement ratio to riser displacement.

of trench shape are finally taken to be: $\lambda = 122$, $\varphi = 0.27$ and $\beta = 0.016$, respectively.

Figs. 11 and 12 show the trench shape for oil and gas export SCR respectively. It can be found that the linear zone is in good agreement, whereas the nonlinear zone depth is slightly over estimated. Overall, the obtained trench shape is satisfactory, and it will improve the prediction accuracy of the fatigue damage near TDP since whether or not considering the trench has a considerable effect on the prediction result [24].

For the proposed linear hysteretic SCR–soil interaction model, it is not comparable with the published experimental [39] and numerical [40] models without accounting for an initial trench. Therefore,

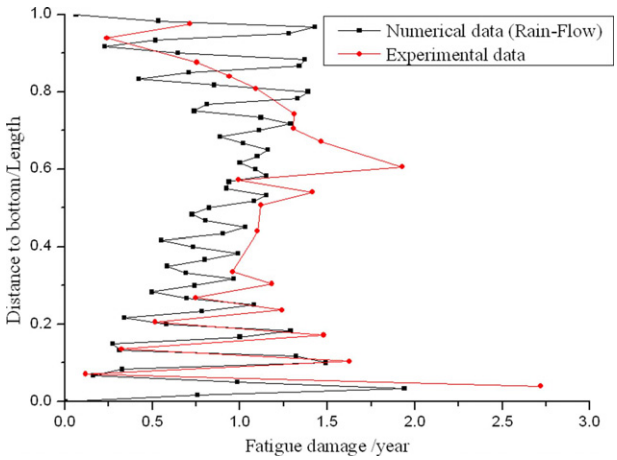

Fig. 10. Fatigue damage per year along the riser model.

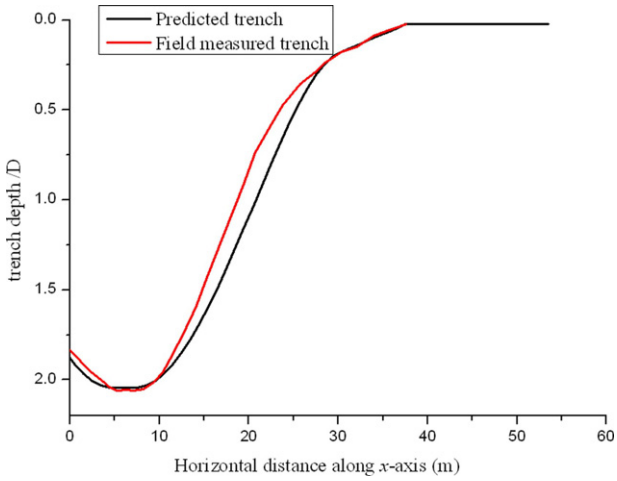

Fig. 11. Comparison of trench shape for oil export SCR.

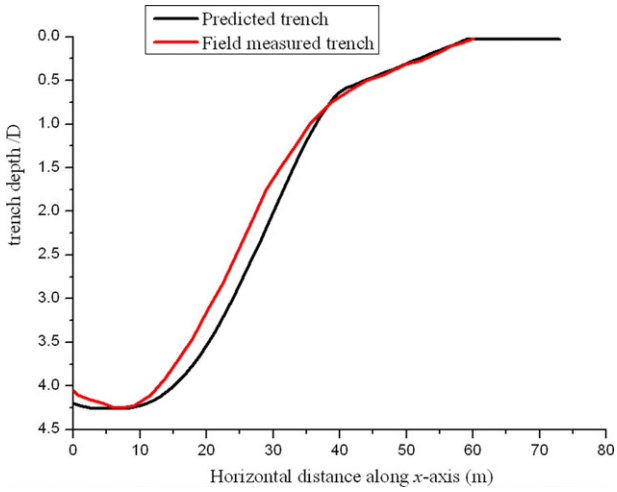

Fig. 12. Comparison of trench shape for gas export SCR.

this study qualitatively discusses the proposed model by modeling the targeted SCR. The riser principles and the related current are presented in the next section, see Table 2 and Fig. 14, respectively. The parameters of the SCR–soil interaction model are: $|z|_{max} = 0.6$ m, $S_0 = 3.5$ kPa, $S_g = 2.5$ kPa/m, $\mu_{sep} = 0.6$, $\lambda_{suc} = 0.8$, $f_{suc} = 0.2$, $\gamma = 122$, $\varphi = 0.27$, $\beta = 0.016$.

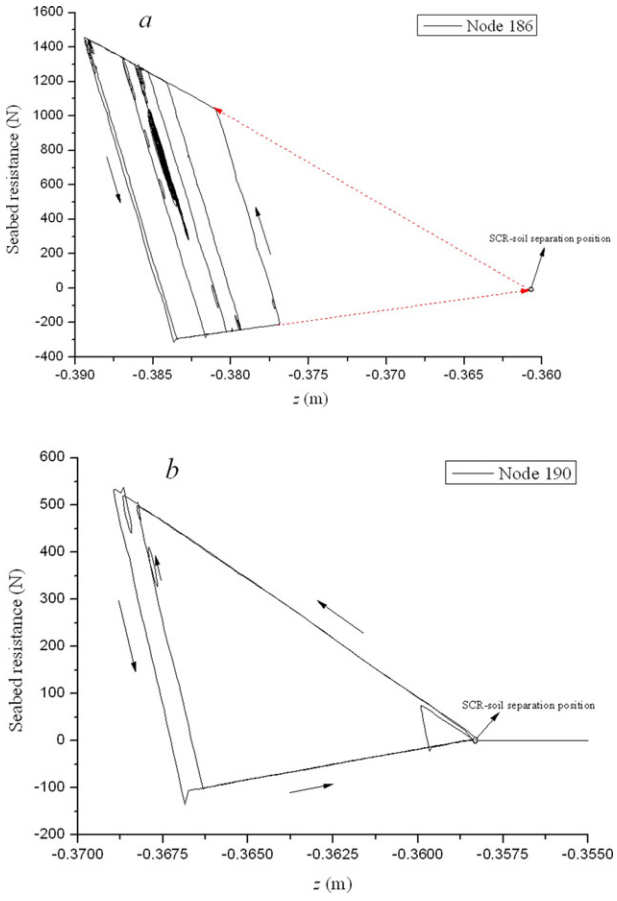

Fig. 13. Seabed resistance vs. penetration for node 186 (a) and node 190 (b).

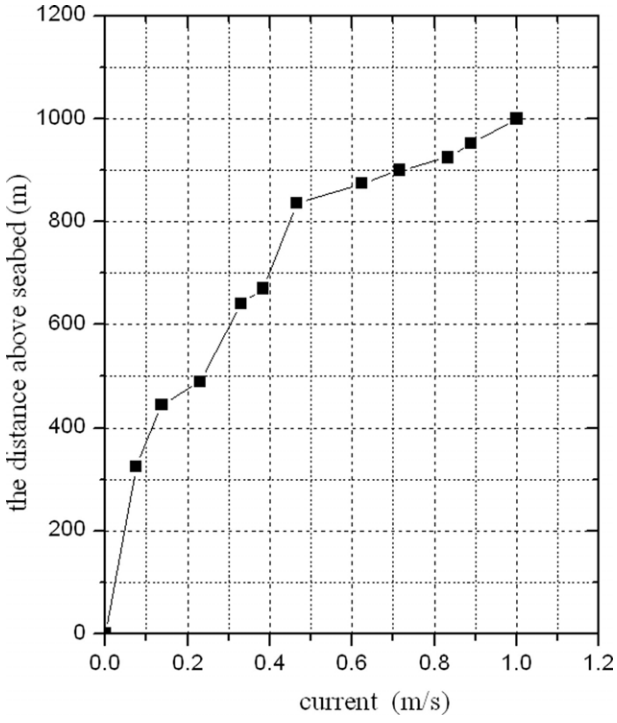

Fig. 14. Current profile.

The length of the SCR elements at TDZ is set to be 1m. By matching the trench shape predicted using the trench model with the static configuration of the SCR, the positions of the maximum trench depth and SCR–soil separation (i.e. TDP) are identified at nodes 186 and 192 respectively (numbered from the bottom end). The seabed resistance profiles as function of penetration at nodes 186 and 190 are illustrated in Fig. 13a and b, respectively. It is shown that node 186 turns to moving downwards without separation with the seabed, accompanied with soil suction reduction and then switching to resistance following the double dot dash line ⑤. Node 190 has more severe response, and separates from and then penetrates the seabed repeatedly. Both figures demonstrate that in a full loop, the maximum soil suction is about 0.2 maximum resistance as expected due to the role of f_{suc}. Overall, the proposed SCR–soil interaction model can reasonably simulates the mobilization and release of the seabed suction.

Table 2
Principles of the targeted SCR.

Length	1410.8	m
Horizontal span	791	m
D_{out}	0.3	m
D_{in}	0.268	m
Mass per unit length	112	kg
Height of top hang off point	975	m
Hang off angle	12	deg

Table 3
Summery of seabed parameter values.

Parameters	Case number		
	1	2	3
$\|z\|_{max}$	0.6	0.6	0.6
S_0	1.0, 2.0, 3.0, 3.5	1.5	1.5
S_g	2.5	1.5, 2.5, 3.5, 4.5	2.5
μ_{sep}	0.6	0.6	0.6
λ_{suc}	0.8	0.8	0.8
f_{suc}	0.2	0.2	0.2,0.25, 0.3, 0.4, 0.6
γ	122	122	122
φ	0.22	0.22	0.22
β	0.15	0.15	0.15

6. Fatigue sensitivity analysis

6.1. Model parameters and modal analysis

Based on the proposed methodology, the sensitivity of the VIV induced fatigue damage of SCR near TDP is to be invested. This study targets a SCR with the parameters in Table 2. The associated current profile is shown in Fig. 14.

Three cases with varying: (1) mudline shear strength, (2) shear strength gradient, (3) suction factor, are calculated and discussed. The associated parameters of the SCR–soil interaction model are presented in Table 3.

Due to the assumption that lock-in occurs at the still water natural frequency, the modal analysis is herein carried out. Fig. 15 shows the modal shapes for mode 2, 3 and 4. It is noted that the shapes near TDP is not fixed at the truncation point, *A*. Therefore, the predicted response near TDP is likely to be different from the traditional model. As seen in Fig. 16, natural frequencies are almost not influenced by the existence of TDZ. This indicates that the predicted dominant mode should be the same for the present model and the truncation model.

6.2. Results and discussion

6.2.1. Effect of mudline shear strength

The seabed stiffness has a significant relationship with the mudline shear strength. Firstly, to identify the critical position, the fatigue damage along TDZ is obtained as shown in Fig. 17. Obviously, critical

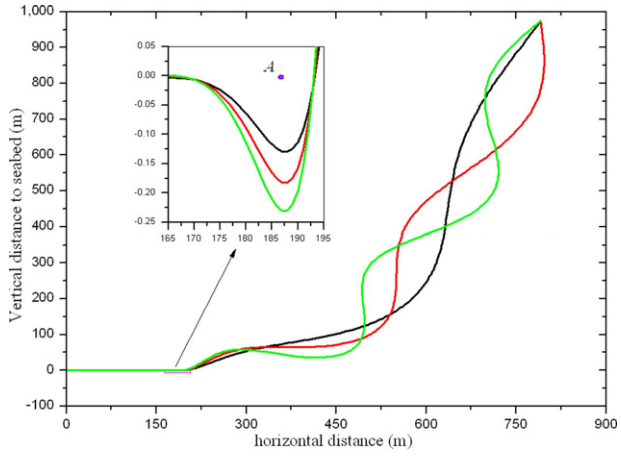

Fig. 15. Modal shapes of targeted SCR.

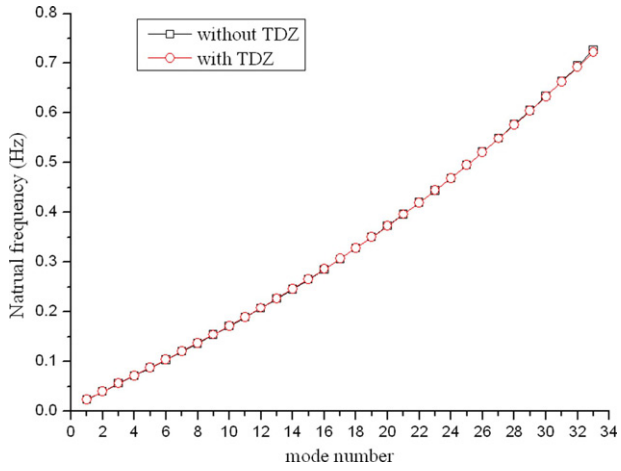

Fig. 16. Natural frequency of targeted SCR (considering added mass).

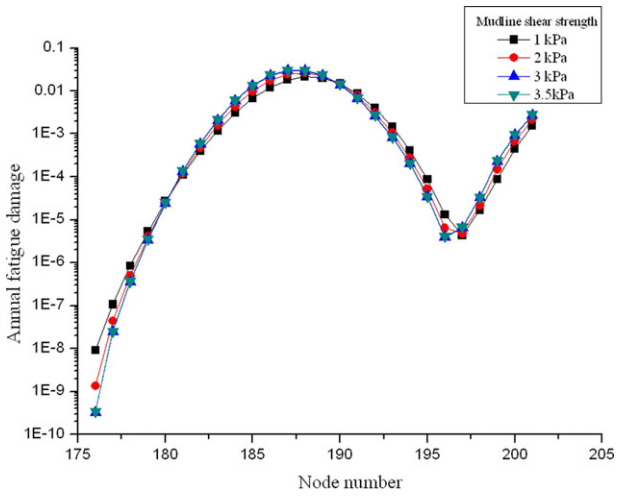

Fig. 17. Annual fatigue damage along TDZ.

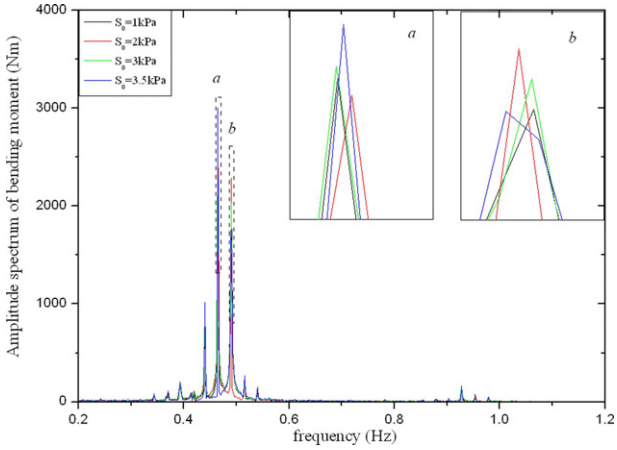

Fig. 18. Amplitude spectrum of bending moment at node 188 for case 1.

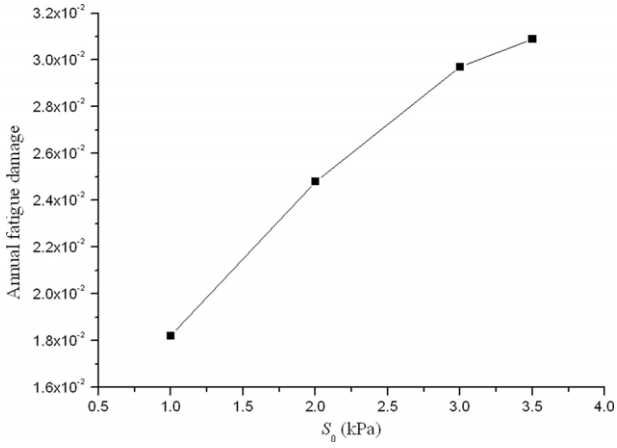

Fig. 19. Annual fatigue damage at node 188 vs. mudline shear strength.

position is near the maximum penetration position (node 186) for this case study, approximately at node 188. In the following content, the related results of node 188 are discussed. The amplitude spectrum of bending moment indicates that three modes 23, 24 and 25, are mainly excited, see Fig. 18. Fig. 18a and b amplify the top location of the spectrum for modes 24 and 25. It can be found that except for the case with $S_0 = 1$ kPa, by increasing S_0, the amplitude creases for mode 24, whereas decreases for mode 25. Additionally, the frequencies of spectrum peaks are slightly different with varying seabed stiffness. The predicted fatigue damage as a function of S_0 is shown in Fig. 19. Higher S_0 corresponding to stiffer seabed gives higher fatigue damage, and lower ratio of fatigue damage to S_0.

6.2.2. *Effect of shear strength gradient*

The effect of S_g on the fatigue damage at the critical position is discussed. Fig. 20 shows that the amplitude of bending moment associated with modes 24 (Fig. 20a) and 25 (Fig. 20b) are not regular. The case with $S_g = 3.5$ kPa/m has largest amplitude for mode 24, whereas has lowest amplitude for mode 25. However, the combination of amplitude in general increases as S_g increases. The fatigue damage is shown in Fig. 21. It indicates that higher S_g as well as higher S_0 leads to higher fatigue damage and lower ratio of fatigue damage to S_g.

6.2.3. *Effect of maximum suction factor*

In this section, the effect of f_{suc} on the vertical displacement and fatigue damage is discussed. Fig. 22 illustrates that increasing suction significantly reduces the peak value, and slightly reduces the valley value. Therefore, higher suction can decrease the motion range and the mean response position. Although the vertical motion range decreases with increasing f_{suc}, the combination of amplitudes associated with modes 24 (Fig. 23a) and 25 (Fig. 23b) overall increases. Therefore, fatigue damage increases with increasing f_{suc}, see Fig. 24.

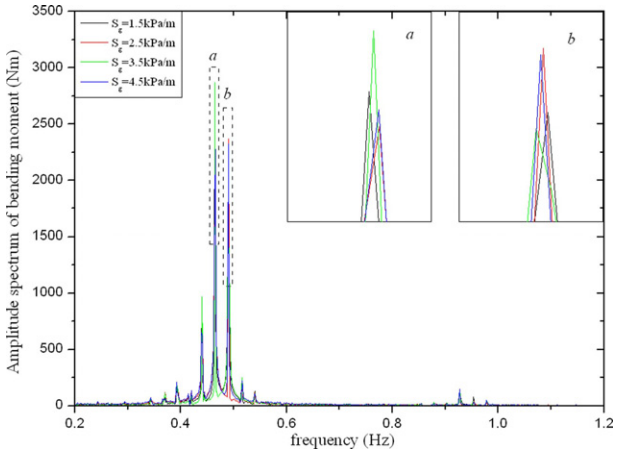

Fig. 20. Amplitude spectrum of bending moment at node 188 for case 2.

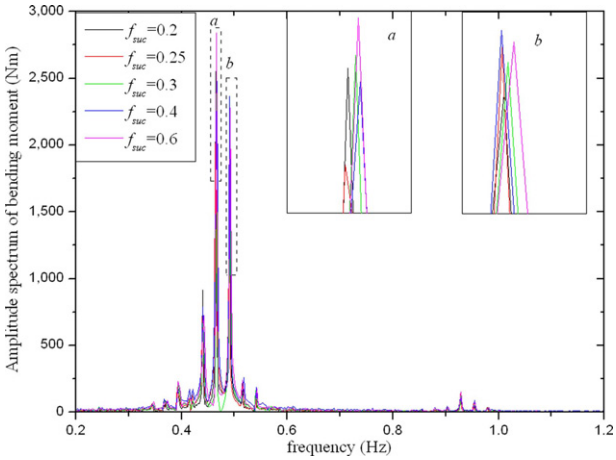

Fig. 23. Amplitude spectrum of bending moment at node 188 for case 3.

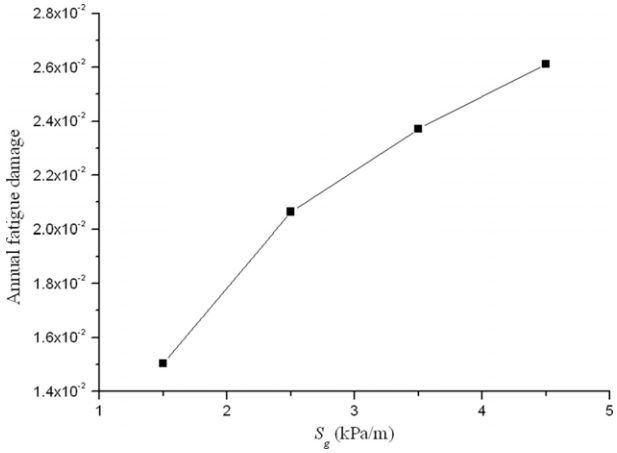

Fig. 21. Annual fatigue damage at node 188 vs. shear strength gradient.

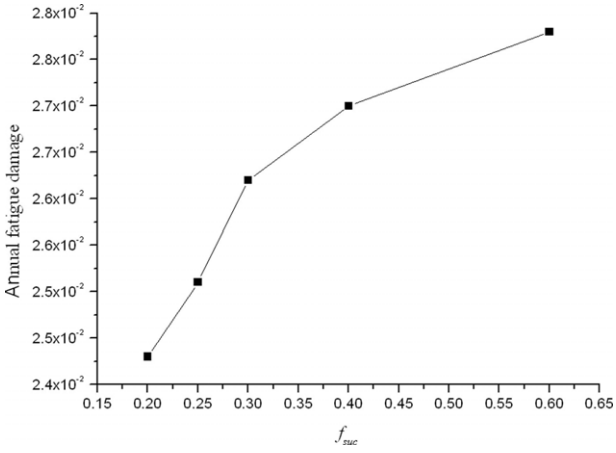

Fig. 24. Annual fatigue damage at node 188 vs. suction factor.

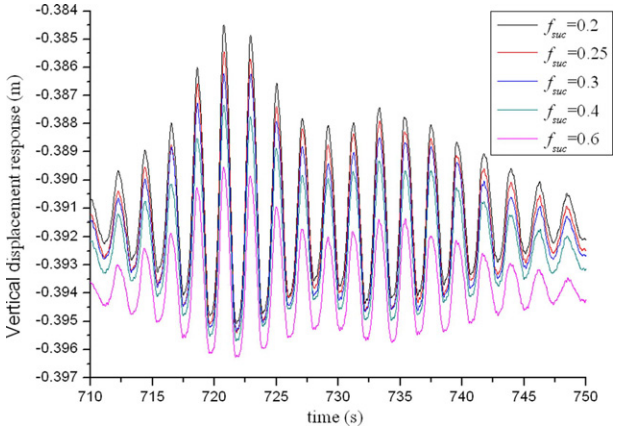

Fig. 22. Vertical displacement time history at node 188.

7. Conclusions

A practical time domain VIV prediction model for SCRs is proposed in this paper. The model can consider the effect of riser-soil interaction based on a new trench shape model, and a linear hysteretic interaction model. The experimentally obtained excitation coefficient and empirical damping model are employed for the hydrodynamic force. The dominant frequency of each riser element depends on the natural frequency, calculated frequency and Strouhal frequency. To validate the new VIV model, a large scale experimental model is simulated. The VIV response and fatigue damage obtained using rain-flow counting method show good agreement with the experimental data. As an attempt, the SCR–soil interaction model taking into account the trench shape is simplified as linear hysteretic model. The trench corresponding to buried zone of a SCR consists of linear and nonlinear zones. It is validated by comparing with the observed trench at Gulf Mexico. As for the linear hysteretic model, due to the lack of comparable numerical and experimental models, only qualitative analysis is carried out. Overall, the proposed models can reasonably predict the VIV response and capture the mobilization and release of seabed suction.

Based on the models, the VIV response of a targeted SCR considering the TDZ is predicted, and the fatigue damage near TDP is obtained using rain-flow methodology. By changing the seabed parameters, parametric studies are carried out, and the following conclusions can be drawn:

(1) Compared with the traditional truncation SCR model, the existence of TDZ does not affect natural frequencies, but affects modal shapes near TDP obviously. The dominant frequency near TDP almost remains constant with the variation of seabed parameters.
(2) This simple case study indicates that the critical position is not the SCR–soil separation position, but between the maximum trench depth position and the SCR–soil separation position.
(3) Higher mudline shear strength and shear strength gradient corresponding to stiffer seabed lead to higher fatigue damage,

and lower ratio of fatigue damage to mudline shear strength and shear strength gradient respectively at the critical position.

(4) Suction decreases the vertical motion span and the mean response position. As the suction increases, the fatigue damage at the critical position slightly increases with reduction of the ratio of fatigue damage to suction factor.

It should be noted that the in-line (IL) VIV and the lateral resistance of the seabed experienced by the SCR is not considered, which are important in SCR design. Therefore, the related investigation would be worthwhile in the future work to broaden the understanding of VIV induced fatigue damage for SCRs.

Acknowledgements

The authors gratefully acknowledge the funding supported by the National Nature Science Foundation of China (Grant No. 51009089) and the Specialized Research Fund for the Doctoral Program of Higher Education of China (Grant No. 20100073120017).

References

[1] Sen TK, Hesar M. Riser soil interaction in soft clay near the touchdown zone. In: Offshore technology conference, Houston, TX, USA. 2007.
[2] Song RX, Stanton P. Advances in deepwater steel catenary riser technology state-of the-art. Part II. Analysis. In: Proceedings of the 28th international conference on ocean, offshore and arctic engineering, Honolulu, Hawaii, USA. 2009.
[3] Sarpkaya T. Fluid forces on oscillating cylinders. Journal of Waterway Port Coastal and Ocean Division ASCE 1978;104:275–90.
[4] Gopalkrishnan R. Vortex induced forces on oscillating bluff cylinders. Cambridge, MA, USA: Department of Ocean Engineering, MIT; 1993.
[5] Govardhan R, Williammson CHK. Modes of vortex formation and frequency response for a freely vibrating cylinder. Journal of Fluid Mechanics 2000;420:85–130.
[6] Vandiver JK, Lee L. User guide for SHEAR7 version 4.2. Cambridge, MA, USA: Massachusetts Institute of Technology; 2002.
[7] Larsen CM, Vikestad K. VIVANA—Theory manual version 3.4. Trondheim, Norway: Norwegian Marine Technology Research Institute; 2005.
[8] Cheng YM, Lambrakos KF. Time domain riser VIV predictions compared to field and laboratory test data. In: Proceedings of the 26th international conference on offshore mechanics and arctic engineering, San Diego, CA, USA. 2007.
[9] Finn L, Lambrakos K, Maher J. Time domain prediction of riser VIV. In: 4th international conference on advances in riser technologies, Aberdeen. 1999.
[10] Grant R, Litton R, Finn L. Highly compliant rigid risers: filed test benchmarking a time domain VIV algorithm. In: Offshore technology conference, Houston, TX, USA. 2000.
[11] Grant R, Litton R, Mamidipudi P. Highly compliant rigid (HCR) model tests and analysis. In: Offshore technology conference, Houston, TX, USA. 1999.
[12] Blevins RD. Flow-induced vibration. New York: van Nostrand Reinhold; 1990.
[13] Cheng YM, Lambrakos KF. Time domain computation of riser VIV from vessel motions. In: Proceedings of the 25th international conference on offshore mechanics and arctic engineering, Hamburg, Germany. 2006.
[14] Cheng YM, Xu LX. Investigation of VIV fatigue prediction for top tensioned riser. In: Proceedings of the 28th international conference on offshore mechanics and arctic engineering, Honolulu, HI, USA. 2009.
[15] Cheng YM, Lambrakos KF. Time domain VIV prediction for top tensioned risers. In: Proceedings of the 29th international conference on offshore mechanics and arctic engineering, Shanghai, China. 2010.
[16] Ma P, Qiu W. Time-domain VIV prediction of marine risers. In: Proceedings of the 31st international conference on offshore mechanics and arctic engineering, Rio de Janiero, Brazil. 2012.
[17] Spencer D., Hui Y, Qiu W. Development and verification of a time-domain VIV simulation tool. In: 3rd international workshop on applied offshore hydrodynamics, Rio, Brazil. 2007.
[18] Spencer D, Leverette S, Masters R. Enabling enhancements of riser VIV design techniques through detailed interpretation of test results for VIV suppression devices. In: Proceedings of the offshore technology conference, Houston, USA. 2007.
[19] Chaplin JR, Bearman PW, Huarte FJH. Laboratory measurements of vortex-indcued vibrations of a vertical tension riser in a stepped current. Journal of Fluids and Structures 2005;21:3–24.
[20] Chaplin JR, Bearman PW, Cheng Y. Blind predictions of laboratory measurements of vortex-induced vibrations of a tension riser. Journal of Fluids and Structures 2005;21:25–40.
[21] Sidarta DE, Finn LD, Maher J. Time domain FEA for riser VIV analysis. In: Proceedings of the 29th international conference on offshore mechanics and arctic engineering, Shanghai, China. 2010.
[22] Wang KP, Tang WY, Xue HX. Time domain analysis approach for riser vortex-induced vibration based on forced vibration test data. In: OMAE2013, Nantes, France. 2013.
[23] Larsen CM, Passano E. Time and frequency domain analysis of catenary risers subjected to vortex induced vibrations. In: Proceedings of the 25th international conference on offshore mechanics and arctic engineering, Hamburg. 2006.
[24] 2H Offshore Engineering Ltd. STRIDE JIP—effect of riser/seabed interaction on SCRs. Report no. 1500-RPT-008; 2002.
[25] Marintek. CARISIMA, interpretation of suction test results. Report No. 700039.00.03, Trondheim, Norway; 2000.
[26] Bridge C, Laver K. Steel catenary riser touchdown point vertical interaction models. In: Offshore technology conference, Houston, TX, USA. 2004.
[27] Aubeny CP, Biscontin G, Zhang J. Seafloor interaction with steel catenary risers. Report. Texas A&M University; 2006.
[28] Nakhaee A, Zhang J. Trenching effects on dynamic behavior of a steel catenary riser. Ocean Engineering 2010;37:277–88.
[29] Wang KP, Xue HX, Tang WY, Guo JT. Fatigue analysis of steel catenary riser at the touch-down point based on linear hysteretic riser–soil interaction model. Ocean Engineering 2013;68:102–11.
[30] Rao ZB, Fu SX, Yang JM. Vortex-induced vibration analysis of steel catenary riser. Journal of Ship Mechanics 2011;15(3):245–58.
[31] Gao Y, Zong Z. Numerical prediction of fatigue damage in steel catenary riser due to vortex-induced vibration. Journal of Hydrodynamics 2011;23(2):154–63.
[32] Meng D, Chen L. Nonlinear free vibrations and vortex-induced vibrations of fluid-conveying steel catenary riser. Applied Ocean Research 2012;34:52–67.
[33] Venugopal M. Damping and response of a flexible cylinder in a current. Cambridge, MA, USA: Department of Ocean Engineering, MIT; 1996.
[34] Sarpkaya T. Fluid forces on oscillating cylinders. Journal of Waterway Port Coastal and Ocean Division ASCE 1978;104:275–90.
[35] Bridge CD, Howells HA. Observations and modeling of steel catenary riser trenches. In: The international ocean and polar engineering conference, Lisbon, Portugal. 2007.
[36] DNV. Fatigue design of offshore steel structures, DNV-RP-C203; 2010.
[37] Baarholm GS, Larsen CM, Lie H. On fatigue damage accumulation from in-line and cross-flow vortex-induced vibrations on risers. Journal of Fluids and Structures 2006;22:109–27.
[38] Lie H, Kaasen KE. Modal analysis of measurements from a large-scale VIV model test of a riser in linearly sheared flow. Journal of Fluids and Structures 2006;22:557–75.
[39] Aubeny C, Gaudin C, Randolph M. . Cyclic tests of model pile in Kaolin. In: Offshore technology conference, Houston, TX, USA. 2008.
[40] Randolph M, Quiggin P. Non-linear hysteretic seabed model for catenary pipeline contact. In: Proceedings of the ASME 28th international conference on ocean offshore and arctic engineering, Honolulu, HI, USA. 2009.